IOP Publishing Semiconductor Science and Technology
Semicond. Sci. Technol. 31 (2016) 125019 (7pp) doi:10.1088/0268-1242/31/12/125019

Moderate bending strain induced semiconductor to metal transition in Si nanowires

M Golam Rabbani[1,3], Sunil R Patil[2] and M P Anantram[1]

[1] Department of Electrical Engineering, University of Washington, Seattle, WA 98195 USA
[2] Department of Physics, College of Engineering, Pune, 411005 MS, India

E-mail: rabbani@uw.edu

Received 1 July 2016, revised 5 October 2016
Accepted for publication 19 October 2016
Published 18 November 2016



Abstract

A moderate amount of bending strains, ~3% is found to be enough to induce the semiconductor-metal transition in Si nanowires of ~4 nm diameter. The influence of bending on silicon nanowires of 1 nm to 4.3 nm diameter is investigated using molecular dynamics and quantum transport simulations. Local strains in nanowires are analyzed along with the effect of bending strain and nanowire diameter on electronic transport and the transmission energy gap. Interestingly, relatively wider nanowires are found to undergo semiconductor-metal transition at relatively lower bending strains. The effect of bending strain on electronic properties is then compared with the conventional way of straining, i.e. uniaxial, which shows that bending is a much more efficient way of straining to enhance the electronic transport and also to induce the semiconductor-metal transition in experimentally realizable Si nanowires.

S Online supplementary data available from stacks.iop.org/SST/31/125019/mmedia

Keywords: nanowire, semiconductor to metal transition, bending stress

(Some figures may appear in colour only in the online journal)

1. Introduction

Silicon nanowires (SiNWs) have been employed in numerous electronic devices (e.g. nanotransistors [1–3], solar cells [4–6]), optoelectronic devices [7], sensors [8–11], as well as thermo-electric energy conversions [12, 13]. They can be fabricated/synthesized in both top-down and bottom-up approaches, with a wide range of diameters; from a few nanometers to a few hundred nanometers. The sub-10 nm diameter nanowires are particularly interesting, as, unlike the bulk silicon and the wider wires, they can have a direct bandgap [14–16]. More interestingly, the bandgap of the narrow SiNW can be efficiently strain engineered [14, 17] to an extent of strain induced reversible direct-to-indirect bandgap transition [14, 15], and also semiconductor to metal transition [18]. This opens up the possibility and realizations of strain-modulated (for not only electronic, but also optoelectronic) properties of SiNWs.

The traditional objective of straining semiconductor devices is to enhance their mobility through lattice mismatch [19, 20] and stress-memorization [21, 22–24] techniques. For NWs though, bending of a substrate containing nanowires [25, 26] or deposition of an extra layer of straining materials [27], such as oxide, nitride and carbide [18], on a part or the entire length of the wire is more common. Bottom-up synthesized nanowires are also unintentionally [28, 29] or intentionally [30], strained and are found to be stable up to over 40% bending strain [31] and with a U-shape bending [32]. In fact it is noted that, as the nanowire diameter decreases, the bending strength increases [32]. These studies [31, 32], indicate that narrow SiNWs, in addition to demonstrating quantum mechanical properties, also offer mechanical stability under large stresses.

When it comes to modeling and simulating the strain effect on electronic properties, there have been numerous attempts, which are usually carried out at the density functional theory (DFT) and classical molecular dynamics (MD)

[3] Author to whom any correspondence should be addressed.

 © 2016 IOP Publishing Ltd Printed in the UK

level [17, 33]. However, owing to the computationally expensive nature of DFT, the device size is usually limited to few 100 s of atoms. Often, the finite size effect is countered by using the periodic boundary condition (PBC). Most of the investigations in this field are therefore limited to uniformly strained material systems. This is largely because non-uniform strain such as bending does not preserve the crystal symmetry, without which PBC cannot be applied along the length of the nanowire. Alternatively, one may consider long enough NWs, which however, increases the computational demand to an unmanageable level. MD can handle larger system sizes and therefore is widely used in the study of mechanical [34, 35] and thermal [36, 37] properties of microscale- [38] as well as nanoscale-devices [39, 40], including silicon nanowires [37, 41–52]. However, only Ponomareva *et al* [52] have studied the effect of bending on the electronic properties of nanowires. On the experimental front, it is understood that bending of NWs increases the conductivity in Si as well as in ZnO and CdS [53, 54]. It is to be noted that bending is not limited to only bottom up nanowires, top-down fabricated nanowires can also be bent intentionally [55, 56] or unintentionally [57, 58]. Moreover, top down and bottom up approaches can be combined [59] to get horizontally suspended, well-oriented and size-controlled nanowire arrays. These bending approaches may open up new possibilities, and thus, further investigations on bent nanowires have become imperative.

Therefore, this work investigates the effect of bending on the electronic properties of SiNWs. Particularly, the approach involves bent SiNWs optimized with MD, and the output (i.e. atomic co-ordinates) is fed to a tight binding model to obtain the electronic Hamiltonian. With this Hamiltonian we perform a quantum transport calculation within the non-equilibrium Green's function [60] formulation. We also present the comparative results of bent nanowires with that of uniaxially strained nanowires. The paper is organized as follows: section 2 describes the simulation methodology followed by section 3, which includes strain analysis, results and discussion on the effect of bending on the electronic properties of NWs, and section 4 is the conclusion section.

2. Methodology

Six different cross-sectional areas, ⟨110⟩ directed SiNWs are studied, as sub-10 nm diameter nanowires grow mainly along the ⟨110⟩ direction [29, 61–65]. The average diameters of the nanowires are 1.0 nm, 1.7 nm, 2.3 nm, 3.1 nm, 3.6 nm and 4.3 nm, which are labeled here as ⟨110⟩2d, ⟨110⟩3d, ⟨110⟩4d, ⟨110⟩5d, ⟨110⟩6d and ⟨110⟩7d, respectively. The total length of each nanowire is 19.922 nm with 103 atomic layers. The initial nanowire structures were generated by the repetition of DFT optimized silicon unit cells [14]. The MD is performed with a Large-scale Atomic/Molecular Massively Parallel Simulator (LAMMPS) [66]. The Tersoff [67, 68] many-body bond-order reactive potential is used to describe the Si–Si interactions. The nanowire structure is first optimized by using energy minimization, with no velocity or force restrictions on any atoms. We follow the bending procedure which was used for bending silicon carbide nanowires [34], where the Si atoms are subdivided into three groups. To apply bending stress to the middle group, the atoms in the left (right) group are rotated counter clockwise (clockwise) in the yz plane (see the supplementary information figure 1(b) top) by an angle of 0.05 degrees. Then, they are kept frozen while energy minimization is done to the middle group of atoms. After minimization, the atomic positions of all the atoms are saved, and the process is repeated for the next increment of the rotation angle. A similar approach is used for uniaxial strain, by shifting the end atoms, instead of rotating them. Since the left and right groups of atoms are kept fixed during the bending or uniaxial straining and energy minimization process, the atoms in the middle group, which are close to atoms in the edge groups, undergo artificial deformations. To avoid this, 19 layers of atoms from each end are cropped off. Next, the remaining 65 layers are hydrogen passivated with the GaussView [69], and then were used for tight binding and quantum transport calculations. We employ the $sp^3d^5s^*$ tight binding (TB) method with parameters from Jancu *et al* [70] to form an electronic Hamiltonian matrix. Without considering spin–orbit coupling in $sp^3d^5s^*$ TB, the Hamiltonian size for each silicon atom is 10×10, and that for each hydrogen atom is 1×1. Thus, the Hamiltonian size of each layer is between 128×128 (for ⟨110⟩2d) and 1498×1498 (for ⟨110⟩7d). The Hamiltonian formed by TB is used to calculate the transmission through the nanowire by using the non-equilibrium Green's function (NEGF) [60] formalism. For ballistic transport, the electronic transmission in a semiconductor is zero in the energy bandgap, therefore, transmission is used to estimate the energy bandgap.

3. Results and discussion

3.1. Strain analysis

In this subsection, we analyze the strains in the nanowires. Figure 1 shows three bent nanowires, (a) ⟨110⟩3d, (b) ⟨110⟩5d, and (c) ⟨110⟩7d, with their local atomic strain along the length (z) direction visualized as color variation. To obtain this strain configuration, the left and right atom groups of each nanowire were rotated by 15° in the vertical (yz) plane. The top side of each nanowire is under tension while the bottom side is under compression. The corner atoms are under the largest amount of strain due to the rotation. Also, for a fixed amount of rotation, as expected, the range of strain variation (from the most compressive to most tensile) increases with the nanowire diameter. In addition, the largest tensile strain magnitude is always higher than the largest compressive strain magnitude, for example, $+3.7\%$ *vs* -2.3% for nanowire ⟨110⟩3d. This is due to the atomic potentials resisting compression more than the tension, because, as the atoms are brought closer to each other beyond the no-strain minimum energy position the energy increases exponentially. We expect the larger diameter nanowires to show an increasingly symmetric strain profile for smaller strains (see

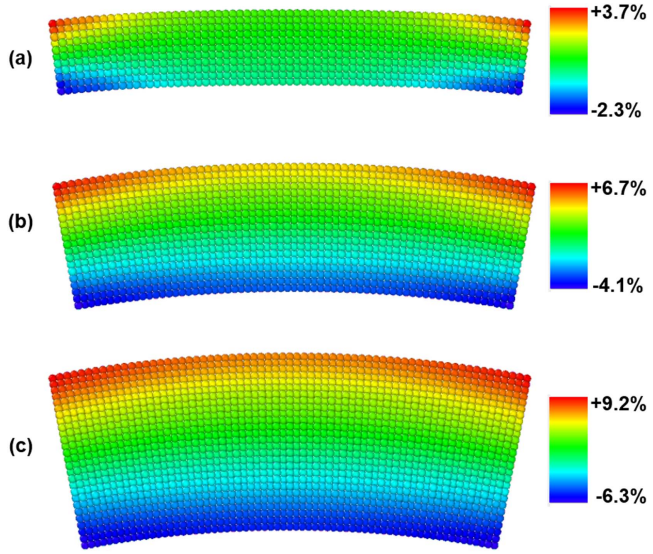


Figure 1. Local strain along the *z*-direction (length) in 3 different nanowires as a color plot; (a) ⟨110⟩3d, (b) ⟨110⟩5d, (c) ⟨110⟩7d.

the supplementary information figure 2), as it is observed experimentally for 30–50 nm diameter nanowires [71].

Figure 2, therefore, plots all the three strain ranges (*x*-range (a), *y*-range (b), and *z*-range (c)) as a function of nanowire diameter for different amounts of end-atom-group rotations. The ranges are almost linearly proportional to the nanowire diameter. The *y*-range values are slightly higher than the *x*-range values as the diameter along *y* is wider. Due to bending along the length, *z*-range values are the largest.

Figures 3(a) and (b) plot the layer-to-layer strain along the length (as defined in equation (1) of the supplementary information), for two different nanowires—(a) ⟨110⟩3d and (b) ⟨110⟩6d. We have already seen in figure 2(c) that the range of variation of *z*-strain over all the atoms in a nanowire can be quite large, mainly because of the corner atoms being under large strain of opposite polarity. However, the layer-to-layer strain variation is actually smaller (figures 3(a) and (b)). As the variation is small, it is possible to find a single quantity, representing an equivalent average strain, for each of the curves in figure 3. This average number is plotted in figure 3(c) for all the bent nanowires considered in this study. For the same end-atom rotation, the average strain increases linearly with the diameter, like the strain ranges. The average strain value is used for studying a correlation with electronic properties and comparison with uniaxially strained nanowires, for which the nominal strain value along the length is used.

3.2. Electronic transmission

In bent nanowires, the bending strain compresses or extends the nanowire locally (figure 1), although on average, the nanowire is under tensile strain along the length (figure 3(c)). The strain (bending or uniaxial) changes the electronic band profile of the nanowire [72]. Due to the absence of crystal symmetry under bending, one cannot determine the energy band structure using the Bloch's theorem. We rather calculate the electronic transmission (supplementary information equation (5)) in the strained nanowires as a function of energy, which has information about the energy gap as well as transmission probability.

Figure 4 shows the electronic transmission through the nanowires as a function of energy for, respectively, zero, 15-degree and 30-degree end-atom-group rotations: (a, b, c) ⟨110⟩2d and (d, e, f) ⟨110⟩7d. We notice three important trends in the plots. First, a narrower nanowire has a lower transmission value. The reason is that a narrower nanowire has fewer number of electronic modes, and, at any energy, transmission is proportional to the number of modes. Second, the transmission gap—the continuous energy range over which the transmission is zero—in the nanowire is larger than the bulk silicon bandgap. As a result of quantum confinement decreasing with increasing NW diameter, the transmission gap decreases as the nanowire diameter increases. The bandgap values, calculated by assuming the entire length of the bent nanowire as a single unit cell, also match with the corresponding transmission gap. In addition, it is to be noted that the gaps in the unstrained nanowires, 2.43 eV (⟨110⟩2d) and 1.43 eV (⟨110⟩7d), are consistent with those obtained with DFT [14] and DFTB [16]. Third and most importantly, the gap in each nanowire decreases as the amount of bending strain (that is, average strain along length) increases. This behavior is also consistent with the results in [14], which

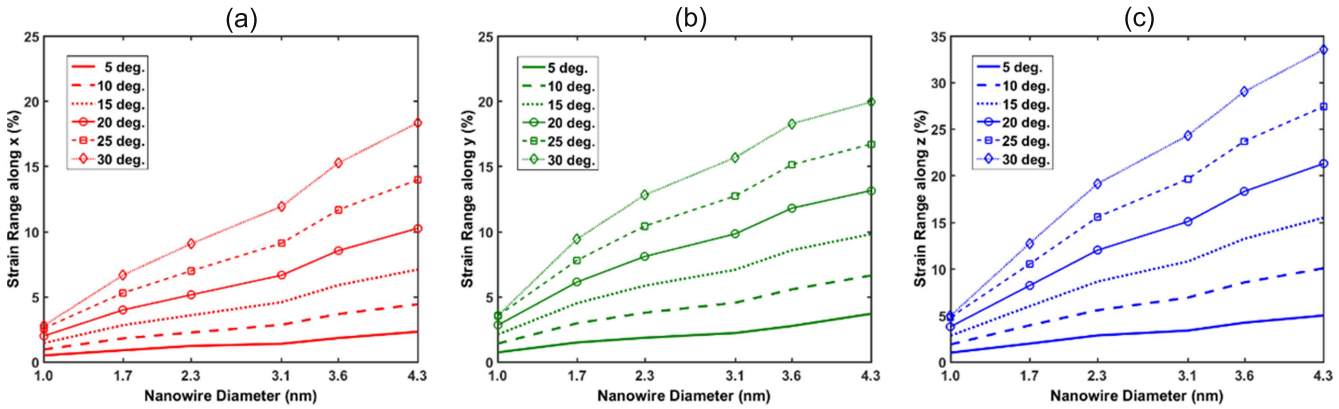


Figure 2. Ranges of strain (*x*-range (a), *y*-range, (b) and *z*-range (c)) as functions of nanowire diameter for different amounts of end-atom-group rotations. *x* and *y* directions are in the cross-sectional plane while *z* is along the length. The *x* dimension is smaller than the *y* dimension. For each case, the bottom curve is for the smallest rotation (5 deg.) and the rotation increases upwards.

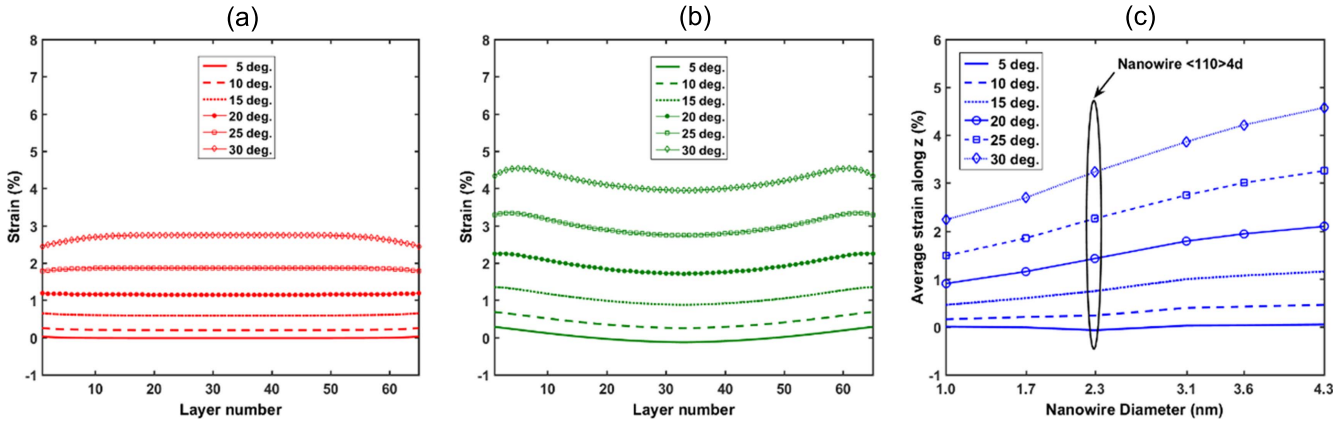


Figure 3. Layer-to-layer average strain along length: (a) ⟨110⟩3d, and (b) ⟨110⟩6d. (c) Average strain along the length as a function of diameter for all six nanowires. Nanowire ⟨110⟩4d has been pointed out.

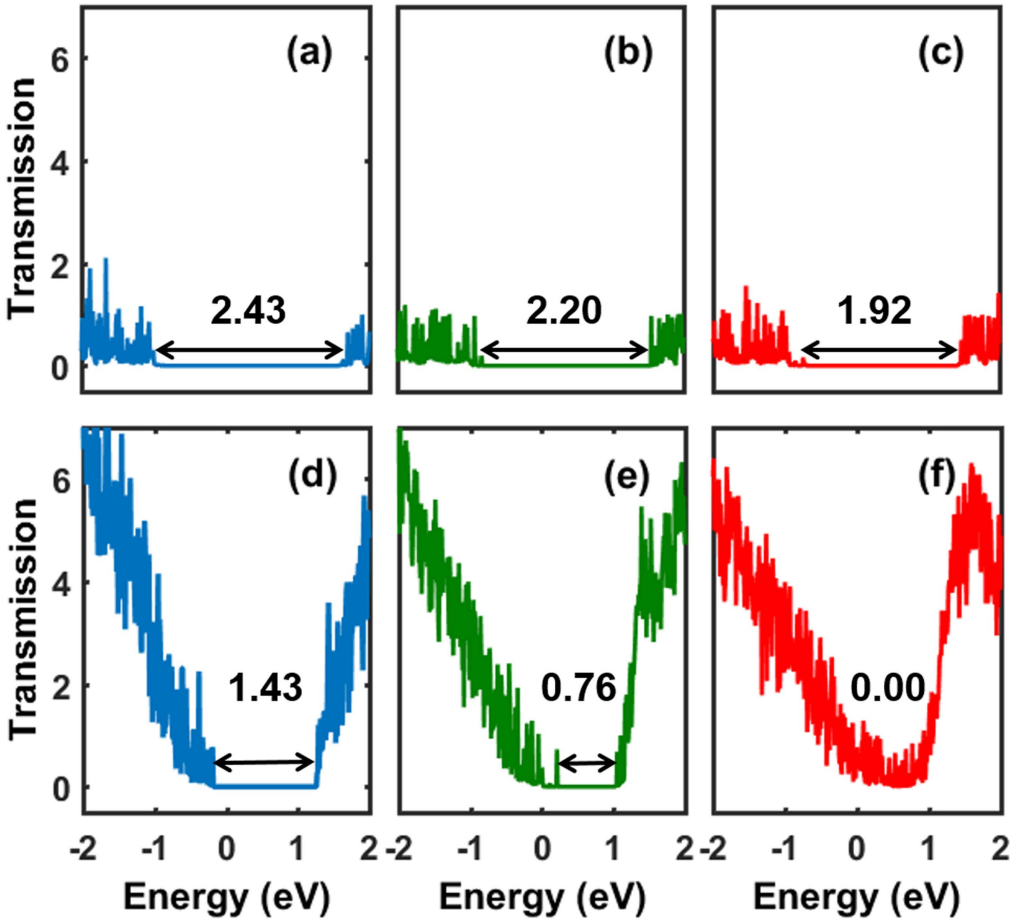


Figure 4. Electronic transmission through two nanowires as a function of energy for different bending angles. Narrowest ⟨110⟩2d nanowire with no rotation (a), with 15-degree rotation (b), with 30-degree rotation (c). Widest ⟨110⟩7d nanowire with no rotation (d), with 15-degree rotation (e), 30-degree rotation (f).

predict that for an increase in uniaxial tensile strain in the nanowire, its bandgap decreases.

We can get a more comprehensive overview by studying the transmission energy gap as a function of the nanowire diameter with the angle of end atom group rotation as a parameter. Such characteristics are plotted in figure 5 for no rotation and six different rotations (5, 10, 15, 20, 25, and 30 degree) conditions (solid lines). For small end-atom rotations (top curves), as the nanowire diameter decreases from the largest diameter, 4.3 nm, the gap increases gradually. This increase, however, becomes sharper as the diameter decreases below 1.7 nm. For large rotations, the gap increases almost linearly as the diameter decreases. It is interesting to note that for the two widest wires, diameters 3.6 nm and 4.3 nm, the gap completely disappears for large strains ∼3%, as the strain range is higher for the wider wires. For large bending, the

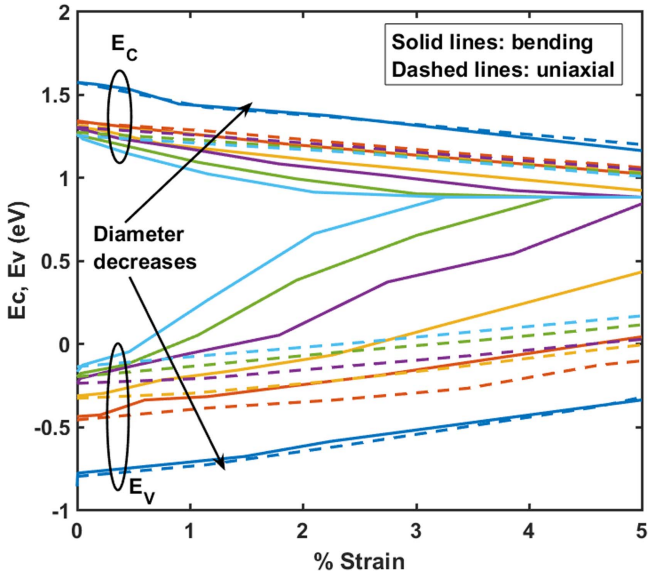


Figure 5. E_C and E_V as a function of % strain. Solid: bent, dashed: uniaxial.

local strains (both tensile and compression) in some parts of the wider wires are very high (and of opposite direction). These large local strains represent a huge departure from the perfect crystal structure and introduce many electronic modes in the band gap, thereby making the gap totally disappear (figure 4(f)). It is to be noted that the uniaxial tensile and compressive strains do not change the crystal symmetry under rotation by an angle that depends on the nanowire diameter, whereas bending removes existing crystal symmetry under rotation, which particularly makes bending an efficient way to tune the band gap. This particular phenomena has been reported in relatively thinner core–shell Si-SiC NWs and attributed to the relatively huge compressive strain ~9% [18]. It has been shown experimentally that bending increases nanowire conductivity [53, 54], so bandgap decrease and conductivity increase can be correlated.

3.3. Bent nanowire vs. uniaxially strained nanowire

Figure 5 also shows the energy gap in electronic transmission as a function of strain for six nanowire uniaxially strained cases (dashed lines). The gap decreases linearly with the strain for both methods of straining, which agrees with uniaxially strained nanowires studied with DFT [14]. However, for the same diameter and the same average strain, the gap is smaller and its decrease rate is faster in the bent nanowires. The larger decrease rate also means that the strain modulated band gap will respond to a wider electromagnetic spectrum. This is clearly an advantage of the bent nanowire over the uniaxially strained nanowire.

It is also to be noted that, for narrow nanowires, both E_C and E_V change at a similar rate, but as the nanowire diameter increases, the rate of change of E_V becomes faster, indicating that the bending affects the valence band maxima more significantly than that of the conduction band minima which is also consistent with [18], where similar observations are noted under relatively large compressive strains of ~9%. Similar trends are seen in bi-axially strained silicon and have been attributed to valence band valley splitting in the effective mass approach [72]. This intricate behavior requires additional investigation, to pin-point the particular phenomenon leading to the significant upward shift in the valence band edge due to the complicated bending strain profile.

We would also like to note here that, although the maximum value of experimentally observed uniaxial strain is about 5% [27], nanowires have been found to withstand large (40%) bending strain [31]. In another study, a U-shape bent 40 nm diameter silicon nanowire was stable up to 11.5% strain [32]. So considering the E_C and E_V trends *vs* strain in figure 5 and the amount of experimentally observed bending, strain can be easily achieved experimentally in SiNWs.

4. Conclusion

Electronic transport properties of SiNWs with diameters from 1 nm to 4.3 nm under bending strain are simulated using MD for structural optimization and NEGF for transport calculations. It is observed that for the same amount of bending, strain range increases with nanowire diameter. The larger strains directly translate into smaller energy gaps in electronic transmission for wider wires. The electronic transport in bent SiNWs are also compared with that which are uniaxially strained. Bending is found to be a more efficient way of tuning the transmission gap compared to uniaxial strain, particularly in shifting the valence band maxima, and enhancing the charge transport, such that SiNWs undergo semiconductor to metal transition at relatively lower strain values. This makes bending an efficient straining mechanism over uniaxial in nanowires with respect to conductance enhancements as well as modulation of energy gaps to exploit the wider electromagnetic spectrum.

Acknowledgments

The work of M Golam Rabbani and M P Anantram was supported by the National Science Foundation under grant no. 1001174 and the QNRF grant (NPRP 5-968-2-403). Sunil R Patil was supported by University Grants Commission: F.5-50/2014(IC).

References

[1] Larrieu G and Han X-L 2013 Vertical nanowire array-based field effect transistors for ultimate scaling *Nanoscale* **5** 2437–41
[2] Colinge J-P *et al* 2010 Nanowire transistors without junctions *Nat. Nanotechnol.* 225–9
[3] Singh N *et al* 2006 Ultra-narrow silicon nanowire gate-all-around CMOS devices: impact of diameter, channel-orientation and low temperature on device performance *2006 Int. Electron Devices Meeting* pp 1–4

[4] Tsakalakos L, Balch J, Fronheiser J, Korevaar B A, Sulima O and Rand J 2007 Silicon nanowire solar cells *Appl. Phys. Lett.* **91** 233117

[5] Adachi M M, Anantram M P and Karim K S 2013 Core–shell silicon nanowire solar cells *Sci. Rep.* **3** 1546

[6] Garnett E and Yang P 2010 Light trapping in silicon nanowire solar cells *Nano Lett.* **10** 1082–7

[7] Li L, Yang C, Junhui H and Qiaowen Y 2013 Preparation and optoelectronic applications of silicon nanowire arrays *Prog. Chem. Rev.* **25** 248–59

[8] Gao Z, Agarwal A, Trigg A D, Singh N, Fang C, Tung C-H, Fan Y, Buddharaju K D and Kong J 2007 Silicon nanowire arrays for label-free detection of DNA *Anal. Chem.* **79** 3291–7

[9] Zheng G, Patolsky F, Cui Y, Wang W U and Lieber C M 2005 Multiplexed electrical detection of cancer markers with nanowire sensor arrays *Nat. Biotechnol.* **23** 1294–301

[10] Park I, Li Z, Pisano A P and Williams R S 2010 Top-down fabricated silicon nanowire sensors for real-time chemical detection *Nanotechnology* **21** 15501

[11] Chua J H, Chee R-E, Agarwal A, Wong S M and Zhang G-J 2009 Label-free electrical detection of cardiac biomarker with complementary metal-oxide semiconductor-compatible silicon nanowire sensor arrays *Anal. Chem.* **81** 6266–71

[12] Dávila D, Tarancón A, Fernández-Regúlez M, Calaza C, Salleras M, San Paulo A and Fonseca L 2011 Silicon nanowire arrays as thermoelectric material for a power microgenerator *J. Micromech. Microeng.* **21** 104007

[13] Stranz A, Kähler J, Merzsch S, Waag A and Peiner E 2011 Nanowire silicon as a material for thermoelectric energy conversion *Microsyst. Technol.* **18** 857–62

[14] Shiri D, Kong Y, Buin A and Anantram M P 2008 Strain induced change of bandgap and effective mass in silicon nanowires *Appl. Phys. Lett.* **93** 73114

[15] Yang X B and Zhang R Q 2008 Indirect-to-direct band gap transitions in phosphorus adsorbed ⟨112⟩ silicon nanowires *Appl. Phys. Lett.* **93** 173108

[16] Nolan M, O'Callaghan S, Fagas G, Greer J C and Frauenheim T 2007 Silicon nanowire band gap modification *Nano Lett.* **7** 34–8

[17] Shiri D, Verma A, Selvakumar C R and Anantram M P 2012 Reversible modulation of spontaneous emission by strain in silicon nanowires *Sci. Rep.* **2** 461

[18] Amato M and Rurali R 2015 Shell-thickness controlled semiconductor-metal transition in Si-SiC core–shell nanowires *Nano Lett.* **15** 3425–30

[19] Patil S R and Melnik R V N 2009 Coupled electromechanical effects in II–VI group finite length semiconductor nanowires *J. Phys. D.: Appl. Phys.* **42** 145113

[20] Patil S, Hong W P and Park S H 2008 Strain fields in arbitrary shaped quantum wires *Phys. Lett.* A **372** 4076–9

[21] Thompson S E *et al* 2004 A logic nanotechnology featuring strained-silicon *IEEE Electron Device Lett.* **25** 191–3

[22] Ortolland C, Okuno Y, Verheyen P, Kerner C, Stapelmann C, Aoulaiche M, Horiguchi N and Hoffmann T 2009 Stress memorization technique—fundamental understanding and low-cost integration for advanced CMOS technology using a nonselective process *IEEE Trans. Electron Devices* **56** 1690–7

[23] Wei A *et al* 2007 Multiple stress memorization in advanced SOI CMOS technologies *2007 IEEE Symp. on VLSI Technology* pp 216–7

[24] Ortolland C, Morin P, Chaton C, Mastromatteo E, Populaire C, Orain S, Leverd F, Stolk P, Boeuf F and Arnaud F 2006 Stress memorization technique (SMT) optimization for 45 nm CMOS *2006 Symp. on VLSI Technology. Digest of Technical Papers* **51** 2005–6

[25] He R and Yang P 2006 Giant piezoresistance effect in silicon nanowires *Nat. Nanotechnol.* **1** 42–6

[26] Arkan E F, Sacchetto D, Yildiz I, Leblebici Y and Alaca B E 2011 Monolithic integration of Si nanowires with metallic electrodes: NEMS resonator and switch applications *J. Micromech. Microeng.* **21** 125018

[27] Passi V, Bhaskar U, Pardoen T, Södervall U, Nilsson B, Petersson G, Hagberg M and Raskin J-P 2012 High-throughput on-chip large deformation of silicon nanoribbons and nanowires *J. Microelectromech. Syst.* **21** 822–9

[28] Hofmann S, Ducati C, Neill R J, Piscanec S, Ferrari A C, Geng J, Dunin-Borkowski R E and Robertson J 2003 Gold catalyzed growth of silicon nanowires by plasma enhanced chemical vapor deposition *J. Appl. Phys.* **94** 6005

[29] Cui Y, Lauhon L J, Gudiksen M S, Wang J and Lieber C M 2001 Diameter-controlled synthesis of single-crystal silicon nanowires *Appl. Phys. Lett.* **78** 2214

[30] Molnar W, Lugstein A, Pongratz P, Seyring M, Rettenmayr M, Borschel C, Ronning C, Auner N, Bauch C and Bertagnolli E 2013 A general approach toward shape-controlled synthesis of silicon nanowires *Nano Lett.* **13** 21–5

[31] Dai S, Zhao J, Xie L, Cai Y, Wang N and Zhu J 2012 Electron-beam-induced elastic-plastic transition in Si nanowires *Nano Lett.* **12** 2379–85

[32] Stan G, Krylyuk S, Davydov A V, Levin I and Cook R F 2012 Ultimate bending strength of Si nanowires *Nano Lett.* **12** 2599–604

[33] Tuma C and Curioni A 2010 Large scale computer simulations of strain distribution and electron effective masses in silicon ⟨100⟩ nanowires *Appl. Phys. Lett.* **96** 193106

[34] Makeev M, Srivastava D and Menon M 2006 Silicon carbide nanowires under external loads: An atomistic simulation study *Phys. Rev.* B **74** 165303

[35] Zhang J, Wang C, Chowdhury R and Adhikari S 2012 Small-scale effect on the mechanical properties of metallic nanotubes *Appl. Phys. Lett.* **101** 93109

[36] Howell P C 2012 Comparison of molecular dynamics methods and interatomic potentials for calculating the thermal conductivity of silicon *J. Chem. Phys.* **137** 224111

[37] Diao J, Srivastava D and Menon M 2008 Molecular dynamics simulations of carbon nanotube/silicon interfacial thermal conductance *J. Chem. Phys.* **128** 164708

[38] Keten S, Chou C-C, van Duin A C T and Buehler M J 2012 Tunable nanomechanics of protein disulfide bonds in redox microenvironments *J. Mech. Behav. Biomed. Mater.* **5** 32–40

[39] Zhang Y Y, Pei Q X and Wang C M 2012 Mechanical properties of graphynes under tension: A molecular dynamics study *Appl. Phys. Lett.* **101** 81909

[40] Hu M and Poulikakos D 2012 Si/Ge superlattice nanowires with ultralow thermal conductivity *Nano Lett.* **12** 5487–94

[41] He Y and Galli G 2012 Microscopic origin of the reduced thermal conductivity of silicon nanowires *Phys. Rev. Lett.* **108** 215901

[42] Guénolé J, Godet J and Brochard S 2011 Deformation of silicon nanowires studied by molecular dynamics simulations *Model. Simul. Mater. Sci. Eng.* **19** 74003

[43] Yang Z, Lu Z and Zhao Y-P 2009 Shape effects on the yield stress and deformation of silicon nanowires: A molecular dynamics simulation *J. Appl. Phys.* **106** 23537

[44] Kang K and Cai W 2010 Size and temperature effects on the fracture mechanisms of silicon nanowires: molecular dynamics simulations *Int. J. Plast.* **26** 1387–401

[45] Brun T, Mercier D, Koumela A, Marcoux C and Duraffourg L 2012 Silicon nanowire based Pirani sensor for vacuum measurements *Appl. Phys. Lett.* **101** 183506

[46] Hochbaum A I, Chen R, Delgado R D, Liang W, Garnett E C, Najarian M, Majumdar A and Yang P 2008 Enhanced thermoelectric performance of rough silicon nanowires *Nature* **451** 163–7

[47] Agarwal A, Buddharaju K, Lao I K, Singh N, Balasubramanian N and Kwong D L 2008 Silicon nanowire sensor array using top–down CMOS technology *Sensors Actuators* A **145–146** 207–13
[48] Chang T-M, Weng C-C and Huang M-J 2010 A nonequilibrium molecular dynamics study of in-plane thermal conductivity of silicon thin films *J. Electron. Mater.* **39** 1616–20
[49] Zhao H and Aluru N R 2009 Size and surface orientation effects on thermal expansion coefficient of one-dimensional silicon nanostructures *J. Appl. Phys.* **105** 104309
[50] Hong B and Panagiotopoulos A Z 2012 Molecular dynamics simulations of silica nanoparticles grafted with poly(ethylene oxide) oligomer chains *J. Phys. Chem.* B **116** 2385–95
[51] Zhang N *et al* 2011 Deformation mechanisms in silicon nanoparticles *J. Appl. Phys.* **109** 63534
[52] Ponomareva I, Menon M, Srivastava D and Andriotis A N 2005 Structure, stability, and quantum conductivity of small diameter silicon nanowires *Phys. Rev. Lett.* **95** 265502
[53] Han X, Jing G, Zhang X, Ma R, Song X, Xu J, Liao Z, Wang N and Yu D 2010 Bending-induced conductance increase in individual semiconductor nanowires and nanobelts *Nano Res.* **2** 553–7
[54] Moselund K E, Najmzadeh M, Member S, Dobrosz P, Olsen S H, Bouvet D, Michielis L D, Pott V, Ionescu A M and Member S 2010 The high-mobility bended n-channel silicon nanowire transistor *IEEE Trans. Electron Devices* **57** 866–76
[55] Zhang S, Lou L and Lee C 2012 Piezoresistive silicon nanowire based nanoelectromechanical system cantilever air flow sensor *Appl. Phys. Lett.* **100** 23111
[56] Yang R, He T, Marcoux C, Andreucci P, Duraffourg L, Feng P X, Engineering E, Western C, Campus M and Cedex G 2013 Silicon nanowire and cantilever electromechanical switches with integrated piezoresistive transducers *IEEE 26th Int. Conf. on Micro Electro Mechanical Systems (MEMS) (20-24 Jan. 2013)* pp 1–4
[57] Pennelli G, Totaro M and Nannini A 2012 Correlation between surface stress and apparent Young's modulus of top-down silicon nanowires *ACS Nano* **6** 10727–34
[58] Rabbani M G 2011 *Cambridge Studies in Semiconductor Physics and Microelectronic Engineering* (Book 3) (Cambridge, UK: Cambridge University Press) pp 1–396
[59] Paulo A S, Arellano N, Plaza J A, He R, Carraro C, Maboudian R, Howe R T, Bokor J and Yang P 2007 Suspended mechanical structures based on elastic silicon nanowire arrays *Nano Lett.* **7** 1100–4
[60] Datta S 1997 *Electronic Transport in Mesoscopic Systems* (*Cambridge Studies in Semiconductor Physics and Microelectronic Engineering*) (Cambridge, UK: Cambridge University Press)
[61] Schmidt V, Wittemann J V and Gösele U 2010 Growth, thermodynamics, and electrical properties of silicon nanowires *Chem. Rev.* **110** 361–88
[62] Eichfeld S M, Hainey M F, Shen H, Kendrick C E, Fucinato E A, Yim J, Black M R and Redwing J M 2013 Vapor-liquid-solid growth of ⟨110⟩ silicon nanowire arrays *Proc. SPIE Nanoepitaxy: Materials and Devices V (19 September 2013)* **8820** 88200I
[63] Wittemann J V, Münchgesang W, Senz S and Schmidt V 2010 Silver catalyzed ultrathin silicon nanowires grown by low-temperature chemical-vapor-deposition *J. Appl. Phys.* **107** 96105
[64] Wu Y, Cui Y, Huynh L, Barrelet C J, Bell D C and Lieber C M 2004 Controlled growth and structures of molecular-scale silicon nanowires *Nano Lett.* **4** 433–6
[65] Huang Z, Shimizu T, Senz S, Zhang Z, Zhang X, Lee W, Geyer N and Go U 2009 Ordered arrays of vertically aligned [110] silicon nanowires by suppressing the crystallographically preferred ⟨100⟩ etching directions *Nano Lett.* **9** 2519–25
[66] Plimpton S 1995 Fast parallel algorithms for short-range molecular dynamics *J. Comput. Phys.* **117** 1–42
[67] Tersoff J 1988 Empirical interatomic potential for silicon with improved elastic properties *Phys. Rev.* B **38** 9902–5
[68] de Brito Mota F, Justo J F and Fazzio A 1999 Hydrogen role on the properties of amorphous silicon nitride *J. Appl. Phys.* **86** 1843
[69] Roy D, Keith T and Millam J 2009 GaussView, version 5, Semichem Inc. Shawnee Mission KS
[70] Jancu J-M, Scholz R, Beltram F and Bassani F 1998 Empirical spds* tight-binding calculation for cubic semiconductors: General method and material parameters *Phys. Rev.* B **57** 6493–507
[71] Zheng K, Han X, Wang L, Zhang Y, Yue Y, Qin Y, Zhang X and Zhang Z 2009 Atomic mechanisms governing the elastic limit and the incipient plasticity of bending Si nanowires *Nano Lett.* **9** 2471–6
[72] Sun Y, Thompson S E and Nishida T 2007 Physics of strain effects in semiconductors and metal-oxide-semiconductor field-effect transistors *J. Appl. Phys.* **101** 1–22